

A METHOD BASED ON BEACH PROFILE ANALYSIS FOR SHORELINE IDENTIFICATION

M. Luppichini^{1,2}, M. Bini¹, A. Berton³, N. Casarosa⁴, S. Merlino⁵, M. Paterni⁶

¹ Department of Earth Sciences, University of Pisa, Via S. Maria, 52, 56126 Pisa, Italy;
monica.bini@unipi.it

² Department of Earth Sciences, University of Study of Florence, Via La Pira 4, Florence, Italy;
marco.luppichini@unifi.it

³ Istituto di Fisiologia Clinica del Consiglio Nazionale delle Ricerche, IFC—CNR,
56124 Pisa (PI), Italy;

paternim@ifc.cnr.it (M.P.); andrea.berton@ifc.cnr.it

⁴ Consorzio di Bonifica C4 BassoValdarno, 56125 Pisa, Italy; nicola.casarosa@c4bassovaldarno.it

⁵ Istituto di Scienze Marine del Consiglio Nazionale delle Ricerche, ISMAR—CNR,
19032 Lerici (SP), Italy;

silvia.merlino@sp.ismar.cnr.it

Abstract – Coastal erosion coupled with human-induced pressure has severely affected the coastal areas of the Mediterranean region in the past and continues to do so with increasing intensity today. In this context, the Pisa coastal plain shows a long history of erosion, which started at the beginning of the nineteenth century. The work aims to provide a method and a software to extract the shoreline position. We apply the Structure from Motion (SfM) techniques to reconstruct a high-resolution Digital Elevation Model using a drone for image acquisition. The algorithm is based on the variation of the topographic beach profile caused by the transition from water to sand. The SfM technique is not efficient when applied to reflecting surfaces like sea water resulting in a very irregular profile over the sea. Taking advantage of this fact, the algorithm searches for the point in the space where a beach profile changes from irregular to regular, causing a transition from water to land. The algorithm is promoted by the release of a QGIS v3.x plugin uploaded on the official repository of the software, which allows the easy application and extraction of other shorelines.

Introduction

In the last years coastal erosion has become one of the main environmental threats worldwide [1]–[4]. About 28 000 km² of the global coastline was eroded between 1984 and 2015 and about twofold as many as those formed by accumulation processes [5]. According to the Fifth Assessment Report of the Intergovernmental Panel on Climate Change (IPCC) [6] the predicted future scenario for coastal zones will deteriorate as a result of the gradual rise in sea level and of the possible surge of extreme events due to current global warming [6]. Specifically, the Mediterranean region is severely affected by the impact of extreme climatic events (e.g., storm surges) joined with human activities (e.g., poorly planned buildings on the coast, dam construction, land use changes inland), resulting in rising vulnerability of the coastal areas [7]. The number of coexisting socio-economic activities (urbanization, tourism, natural protected areas) makes it imperative to understand and further

Referee List (DOI 10.36253/fup_referee_list)

FUP Best Practice in Scholarly Publishing (DOI 10.36253/fup_best_practice)

Marco Luppichini, Monica Bini, Andrea Berton, Nicola Casarosa, Silvia Merlino, Marco Paterni, *A method based on beach profile analysis for shoreline identification*, pp. 47-60 © 2022 Author(s), CC BY-NC-SA 4.0, 10.36253/979-12-215-0030-1.05

monitor coastal dynamics [8]–[11]. Land cover change is considered one of the most important variables of global change affecting the littoral systems, particularly for the effects on river sediment supply [12]–[14]. A reduction in solid load documented for several river-systems of the Mediterranean basin (e.g., Nile, Ebro, Rhône), in particular after the 1970s [8], [13], [15], [16], has been considered one of the main causes of coastal erosion, together with subsidence and sea level rise [9], [17]–[19].

Despite the importance of a correct valuation of solid load, for many Mediterranean rivers solid load measurements are insufficient, probably because they are cost- and time-consuming. For these reasons, the input of solid load in countering coast erosion is largely approximative. Even less data is available about the dynamics of long-shore and off-shore dispersion of sediments carried by rivers.

Currently, the more advanced techniques for littoral monitoring start with the sample of the shoreline, which is the dynamic interface between water and land [20] and, according to Boak and Turner [21], there are two main groups of shoreline indicators: those based on the detection or identification of visible features (e.g., instantaneous water lines, vegetation lines), and those based on the intersection of the coastal profile with a specific elevation datum like the 0m Above Mean Sea Level (AMSL). Different procedures exist for coastal monitoring, which are based on direct and remote acquisition systems. Shoreline acquisitions is normally made by the use of DGPS technique of post-processing or of real-time methodology [22], [23]. The main disadvantage of this technique lies in the time required to cover large coastline stretches. Remote sensing can be distinguished by observation of satellite images [24]–[28], Unmanned Aerial Vehicles (UAV) [29]–[32], video monitoring [33], [34], historic aerial photos, and cartography [35], [36].

Several methods capable of discriminating between sea and land have been proposed to extract shorelines from images. Plant and Holman [37] used a method initially developed for grey-scale cameras, called Shoreline Intensity Maximum (SLIM). Recently, with the adoption of colour cameras, spectral information has also been exploited to identify the shoreline, using the water property to absorb the red signal and the sand property to absorb the green and blue signals [38].

The work aims to propose a new method to recognize the shoreline position based on the beach profile using high resolution Digital Elevation Model (DEM) derived by Structure from Motion (SfM) technique. The algorithm is applicable with the use of a QGIS v 3.x plugin which is composed by a user-friendly interface.

Study area

To investigate the role of different methods in the reconstruction of shorelines, we chose to acquire UAV images and Differential GPS (DGPS) in the littoral area located in the hydrographic right of the Arno River. The stretch of coast studied is about 4.5 km and is located on the right bank of the Arno River.

The Pisa coastal plain has been gradually shaped by the Arno River since the Late Holocene [39]–[42] (Figure 1). In the littoral area located in the hydrographic left of the Arno River the littoral drift is mainly oriented towards the south, with the exception of the area between Calambrone and the Scolmatore Channel, where the littoral drift is oriented towards the north. Conversely, in the littoral sector located in the hydrographic right, the littoral drift is oriented towards the north [11], [40] (Figure 1).

Several previous studies showed that this area is currently affected by erosion. Following a period of progradation due to the phases of Arno delta building beginning at about 3000 ka BP [43]–[47], different parts of the Pisa plain experienced marked coastal erosion, which started at the end of the 19th century and amplified after the construction of the river mouth jetty, especially on the hydrographic right [36], [48]–[51].

The area northward of the Arno River Mouth is particularly affected by erosion, but overall value of erosion remained low until the 1950s when there was a rapid documented increase of the process [51]. Erosion was particularly severe at the end of the 1980s, maybe caused by the effects of dredging/damming [52], [53]. The following period was characterized by an increase in erosion around 2010, while a reduction in the erosion rate has been documented in the last eight years (since 2012). The period most affected by erosion was around the 1980s, while the areas that most experienced this phenomenon are the area northwards of the Morto Nuovo River [49], [51], [54].

The role of solid load in countering the coastal erosion of this territory is recognised by the qualitative anticorrelation between fluvial discharge and erosion rate [51]. In particular, the lower fluvial discharge values occurred in the years 1954, 1978, 2012 corresponding to a peak of erosion, while in the years 1928–1944, 1954–1975, and after 2012 the erosion rate tends to decrease, and the river discharge increased. In the period 1960–2012 the river discharge was significantly low. This was particularly true when the Arno River can transport a significant amount of sediments and this is verified with a discharge $>700 \text{ m}^3/\text{s}$ (referred to the station of San Giovanni alla Vena) [51].

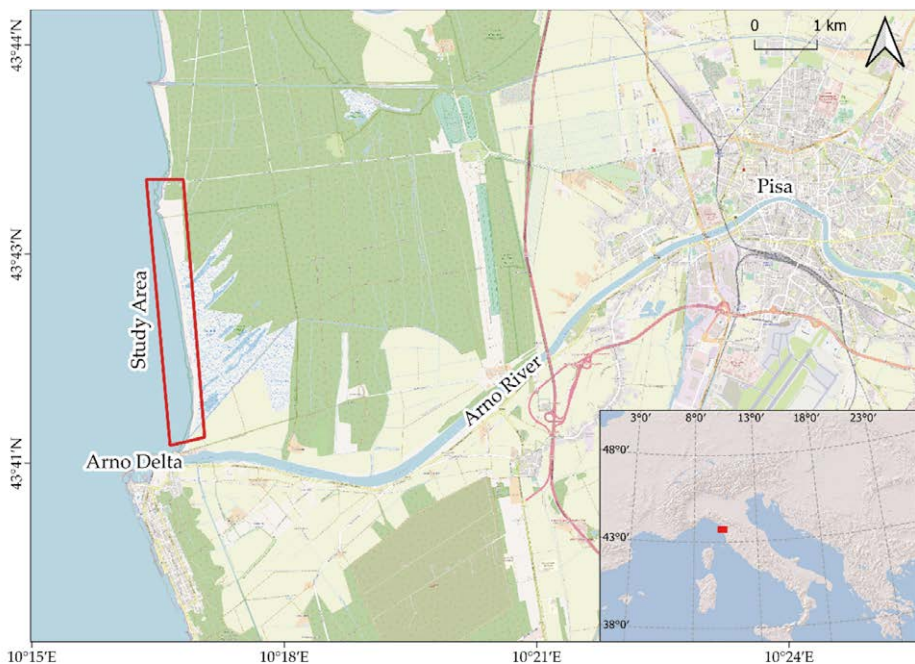


Figure 1 – Location map of the study area.

Materials and Methods

We have acquired 224 points with a R8s Trimble real-time kinematic (RTK) DGPS. The 224 points were divided into pairs, so that the shoreline was sampled by taking a first point in the water and second one on the land where the waves ended [56]. Positioning of the shoreline depends on the elevation of the two investigated DGPS points. In the case that one among the points has a negative elevation and the other one has a positive value; the algorithm makes a linear interpolation between the two acquired points. It selects the point with 0 m of elevation among the interpolate points and it derives the x and y coordinates of the shoreline from this point. In case both points have positive (or negative) elevations, the only difference is that the algorithm selects along the topography profile the point (latitude and longitude) with the coordinate z equal to the mean altimetry of two DGPS points investigated from this point. With this algorithm, we assume AMSL basing on the elevation of the DGPS points. When the 0 m AMSL is included in the topography profile, we consider this altimetry as the most representative of the margin between water and land basing on the definition provided by [21]. When the 0m AMSL is not included in the topography profile, we must choose another AMSL altimetry. In such case, we believe that the best representative altimetry is the mean elevation between the two extremes of the profile (one towards land and the other towards sea).

After the identification of all the 112 points of shoreline, we draw the polyline representing the margin between water and land.

SfM photogrammetry is a technique that allows to reconstruct 3D models starting from a collection of photos of the same elements obtained from different viewpoints [57]–[59]. The frames are sampled by means of an Unmanned Aerial Vehicle (UAV) equipped with a consumer-grade camera.

In particular, we used DJI Phantom 4 Pro V2, which is a quadcopter with a flight autonomy of 30 minutes even if, for safety reasons, we did not exceed 20 minutes of flight. The FC6310S camera was able to take photos of 5472×3648 pixels (in a 3:2 aspect ratio setting).

All acquisitions were obtained with a 24 mm focal length and camera oriented in orthogonal mode with respect to the ground.

The flights were in automatic mode and reached a maximum distance of 500 m from the pilot (as required by the Italian regulatory system), making it possible to perform 1 km sections for each flight.

All flight plans were created using the Desktop UgCS (Universal Ground Control Station) software and were performed using the UgCS application for Android OS. The "Area scan" function allowed us to set the parameters so as to obtain a flight height of 50 m above ground level (AGL) and an overlap of the acquired photos equal to 75 % for each side. By using this flight height, we were able to scan a 75×50 -meter area for each photo. Image acquisition was directly controlled by the flight execution software, UgCS for DJI (Android version); the shooting interval was set to 2 seconds, the manual focus to infinity, while disabling the autoexposure, and storage format was JPG. Four parallel transects were performed for each flight, to obtain a mapping of 1000×70 m with the yaw of the drone constantly set at the same angle with respect to the Earth's North.

The UAV and DPGS samplings were carried out simultaneously; moreover, the area is subject to a small tidal excursion [60]. For this reason, we can consider that the two samples

represent the same situation of the sea and that the results are not affected by a significant change in weather and sea conditions. The results derived by the two methods are comparable to each other.

Georeferencing of the 3D model obtained through SfM requires the identification of the ground control points (GCPs) of already known coordinates. We processed the photos and GCPs by using Metashape Professional software (Agisoft LLC, St. Petersburg, Russia), which implements SfM and multi-view stereo matching algorithms.

GCPs are typically used as control points to optimize camera position and orientation data, making it possible to obtain better model reference results.

To extract the shoreline from DEMs and orthomosaics, we identified a new semi-automatic method based on the beach profile. The method is based on the principle that SfM performs poorly on uniform or reflecting surfaces like the sea [61]. The beach profiles obtained with SfM are more irregular and unrealistic on sea, becoming regular and realistic when the points are referred to the land. The algorithm is based on the use of transects along the beach. The orientation of the transects must have from the water to the land. The profile of the transect, which includes the surface of the sea, will be characterized by a low coefficient of determination (R^2), moving from the sea towards the beach and gradually discarding part of the transect profile, which will be regularized until it includes only and exclusively the beach profile.

When the profile has an R^2 greater than or equal to a determined threshold, the algorithm stops and associates the point of coordinates closest to the sea (for example the shoreline point; Figure 2).

We developed a QGIS v3.x plugin in Python 3 to make the algorithm available to the scientific community working in the field. The plugin can be downloaded with the official repository of QGIS. After installation of the plugin a new icon is visible on the QGIS toolbar: when clicked, an interface is opened (Figure 3). The interface is composed by three tabs: “Run algorithm”, “Information” and “Log”. The first tab allows to set the input used by the algorithm:

- DEM raster requires the topography of the beach;
- Transects layer requires the vector layer of the transects used to calculate the shoreline. The transects must be designed with a sea-land orientation, and they must have an order field;
- Order field is the field of a transect layer that can be both numeric and alphabetic. It is used to process the transects with a specific order by which the shoreline will then be constructed;
- Delta X is the dimension of the step used to analyze the beach profile;
- R2 limit is the limit of R^2 above which you pass from a sea profile to an exclusively beach profile;
- Output Shoreline allows to save the Shapefile result.

By clicking on the “OK” push button, the plugin executes the algorithm. Every error and information on execution of the algorithm are recorded in the “Log” tab.

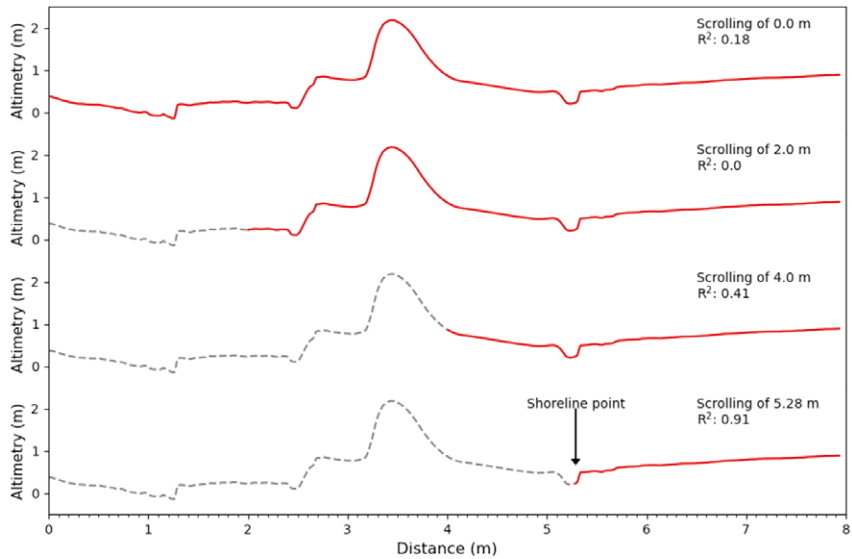


Figure 2 – Description of shoreline identification algorithm. Four illustrative steps of the algorithm to find the shoreline point (from the top to the bottom). R^2 is calculated only on the part of the profile coloured in red. The grey dashed line represents the progressive part of the profile discarded by the algorithm (modified by [62]).

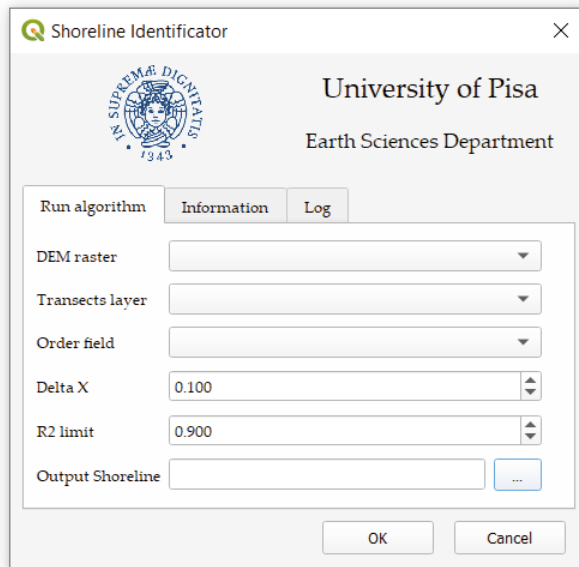


Figure 3 – “Shoreline Identifier” Plugin interface.

Results

The investigated shoreline of about 4.2 km was divided into four flights of UAV. The DEMs have a mean resolution of 2.22 cm/pixel and the entire covered area is 0.44 km².

Figure 4 shows three frames of the shorelines obtained with DGPS points and UAV image processing. The two shorelines are different, but it is difficult to claim whether one is better than the other. The DGPS-derived shoreline in Figure 4a approximates the real shoreline better than the UAV-derived shoreline. However, in Figure 4c, the behaviour is opposite, and in Figure 4b, the two shorelines approximate the real shoreline better alternating.



Figure 4 – Shorelines derived from DGPS points (pink line) and from UAV image processing (orange line). a) The DGPS-derived shoreline (pink line) approximates the real shoreline better than the UAV-derived shoreline (orange line); b) the two shorelines approximate the real shoreline better alternating; c) the UAV-derived shoreline (orange line) approximates the real shoreline better than the DGPS-derived shoreline (pink line) (modified by [62]).

Discussion

We evaluated shoreline extracted by the method proposed in this work comparing with a shoreline derived by DGPS. Figure 4 displays the distances between the relative points of shoreline derived from DGPS and those derived from UAV images. We needed about 8 transects every 100 meters to obtain a minimal error between the two types of shorelines

(Figure 5). The minimal mean error with more than 12 transects/100 m is 1.58 m. The number of transects necessary to obtain a precise shoreline is also influenced by the coastline profile; for example, a more irregular coastline needs a greater number of transects. The advantage of this method is that we can decide the number and position of transects after the survey during the elaboration and this is not possible when we sample the shoreline with a DGPS survey.

Figure 6 shows the differences in terms of areas by comparing the DGPS-derived with the UAV-derived shoreline. The blue areas represent the total area when the DGPS-derived shoreline is less seaward than the other shoreline. The orange areas show the total area, when the DGPS-derived shoreline is more seaward than the other shoreline. The shoreline derived from the UAV images is closer to the beach than the shoreline derived from the DGPS points (Figure 6). The UAV-derived shorelines overestimate the mainland compared to the DGPS-derived shorelines. In some cases, equal to about 30 % of the total investigated area, the UAV-derived shorelines underestimate the mainland compared to the shoreline derived from DGPS (Figure 6).

The Root Mean Square Error (RMSE) between the DGPS shoreline and the UAV-derived shoreline using 12.8 transects/100 m is 1.69 m, much lower than the methods involving the analysis of satellite images, whose order fluctuates between 6 and 12 m depending on the techniques and images used [63]–[65].

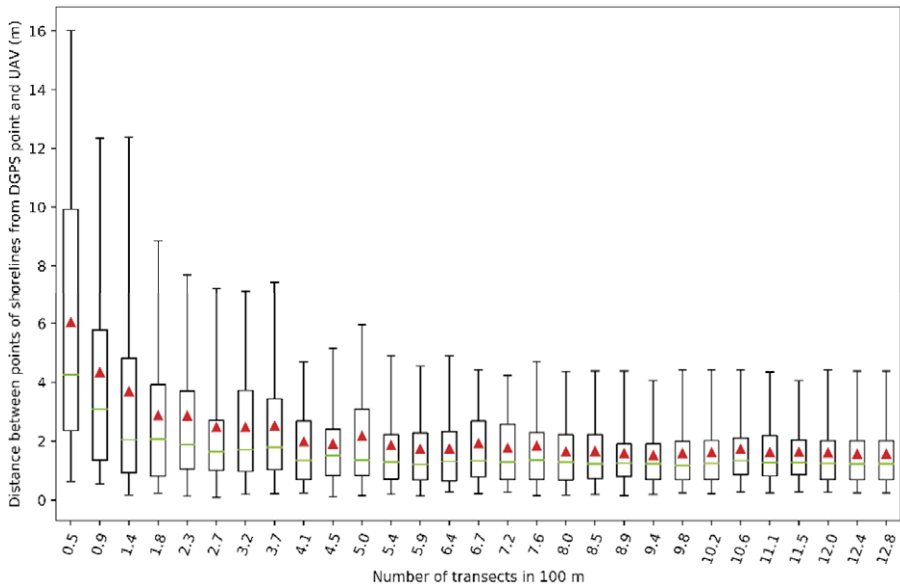


Figure 5 – Analysis of errors between shoreline points derived from DGPS points and those derived from DEM by Structure from Motion (SfM) processing. The box represents the 25th and 95th percentiles, the green line the median, the red triangle the mean, and the whiskers the 5th and 95th percentiles (modified by [62]).

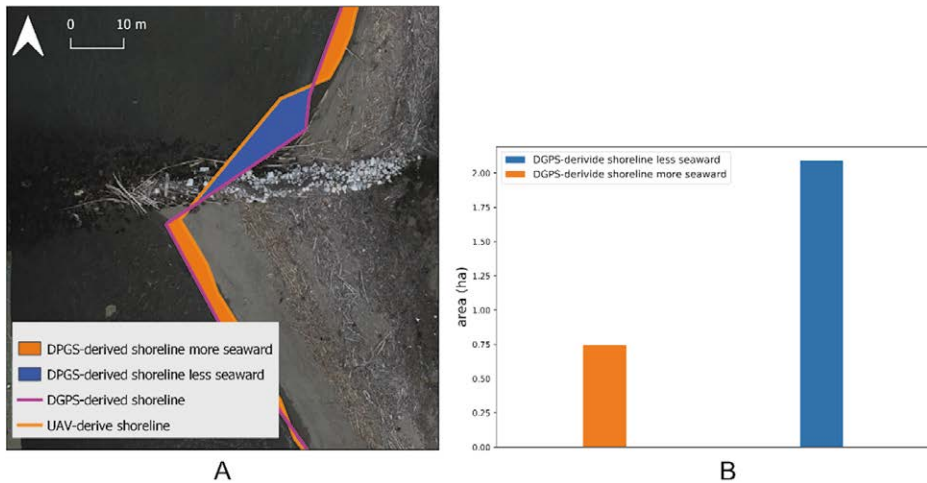


Figure 6 – Analysis of the differences between DGPS-derived shorelines and UAV-derived shorelines. (a) Example of the differences in the areas between DGPS-derived shorelines and UAV-derived shorelines; (b) bar plot of the different areas of the beach comparing the two types of shorelines. The orange and the blue rectangles show the total area when the DGPS-derived shoreline is more or less seaward compared to the other shoreline obtained from UAV images (modified by [62]).

Conclusions

The method proposed in this study is a valid alternative to the classical methods of shoreline identification based on topography. This method makes it possible to obtain shorelines using the topography obtained from UAV images; it is a novelty compared to other uses of DEMs obtained from UAV images present in the literature.

This approach is innovative, and it could also be a valid alternative to the methods based on manual identification or on remote-sensing image colours. In this respect, it is very hard to compare differently-derived shorelines when the errors are about 1–2 m. When we compare the use of satellite images and of DGPS, identification of the error between the two methods is simpler than when we compare the DGPS-derived shoreline with UAV-derived images. This happens because the error of DGPS points to extract the shoreline is negligible compared to the errors that occur when using satellite images with a pixel size of about 10 meters. However, when we compare DGPS-derived shorelines with UAV-derived images, all the errors are of the same order of magnitude. This work has shown that in some cases the DGPS-derived shoreline is better than the UAV-derived shoreline, but in the same number of cases, the roles are reversed. In summary, this new method has two main advantages regarding the use of DGPS points: I) the first advantage is the amount of time it takes to obtain a stretch of coast; ii) the second advantage is that the position of the transects used to reconstruct the shoreline can be decided after sampling and not during acquisition of the DGPS points.

The main disadvantage of this method compared with the DGPS technique is that the second one allows, for time unit, to sample a longer stretch of beach, but, as discussed, with fewer points and consequently with a lower resolution. The use of DGPS allows for a massive sample of the shoreline position.

References

- [1] N. Lenôtre, P. Thierry, D. Batkowski, and F. Vermeersch, "EUROSION project The Coastal Erosion Layer WP 2.6," no. February, p. 45, 2004.
- [2] A. Luijendijk, G. Hagenaars, R. Ranasinghe, F. Baart, G. Donchyts, and S. Aarninkhof, "The State of the World's Beaches," *Scientific Reports*, vol. 8, no. 1, p. 6641, 2018, doi: 10.1038/s41598-018-24630-6.
- [3] IPCC, "Global warming of 1.5°C. An IPCC Special Report on the impacts of global warming of 1.5°C above pre-industrial levels and related global greenhouse gas emission pathways, in the context of strengthening the global response to the threat of climate change," 2018.
- [4] E. C. F. (Eric C. F. Bird, I. G. Union. W. G. on the Dynamics of Coastline Erosion, and I. G. Union. C. on the Coastal Environment, *Coastline changes : a global review*. Chichester (West Sussex] ; New York : Wiley, 1985.
- [5] L. Mentaschi, M. I. Voudoukas, J.-F. Pekel, E. Voukouvalas, and L. Feyen, "Global long-term observations of coastal erosion and accretion," *Scientific Reports*, vol. 8, no. 1, p. 12876, 2018, doi: 10.1038/s41598-018-30904-w.
- [6] IPCC, "Climate change 2013 The Physical Science Basis (eds Stocker, T. F. et al.)," 2013.
- [7] A. Toimil *et al.*, "Climate change-driven coastal erosion modelling in temperate sandy beaches: Methods and uncertainty treatment," *Earth-Science Reviews*, vol. 202, p. 103110, 2020, doi: <https://doi.org/10.1016/j.earscirev.2020.103110>.
- [8] M. Besset, E. J. Anthony, and F. Bouchette, "Multi-decadal variations in delta shorelines and their relationship to river sediment supply: An assessment and review," *Earth-Science Reviews*, vol. 193, no. November 2018, pp. 199–219, 2019, doi: 10.1016/j.earscirev.2019.04.018.
- [9] E. J. Anthony, N. Marriner, and C. Morhange, "Human influence and the changing geomorphology of Mediterranean deltas and coasts over the last 6000years: From progradation to destruction phase?," *Earth-Science Reviews*, vol. 139, pp. 336–361, 2014, doi: <https://doi.org/10.1016/j.earscirev.2014.10.003>.
- [10] E. J. Anthony, "Sand and gravel supply from rivers to coasts: A review from a Mediterranean perspective," *Atti della Societa Toscana di Scienze Naturali, Memorie Serie A*, vol. 125, pp. 13–33, 2018.
- [11] G. Anfuso, E. Pranzini, and G. Vitale, "An integrated approach to coastal erosion problems in northern Tuscany (Italy): Littoral morphological evolution and cell distribution," *Geomorphology*, vol. 129, no. 3, pp. 204–214, 2011, doi: <https://doi.org/10.1016/j.geomorph.2011.01.023>.
- [12] G. P. Petropoulos, G. Ireland, and B. Barrett, "Surface soil moisture retrievals from remote sensing: Current status, products & future trends," *Physics and Chemistry of the Earth, Parts A/B/C*, vol. 83–84, pp. 36–56, 2015, doi:

- <https://doi.org/10.1016/j.pce.2015.02.009>.
- [13] P. Billi and M. Fazzini, “Global change and river flow in Italy,” *Global and Planetary Change*, vol. 155, no. July, pp. 234–246, 2017, doi: <https://doi.org/10.1016/j.gloplacha.2017.07.008>.
- [14] G. Blöschl *et al.*, “Changing climate both increases and decreases European river floods.,” *Nature*, vol. 573, no. 7772, pp. 108–111, Sep. 2019, doi: 10.1038/s41586-019-1495-6.
- [15] J.-P. Degeai *et al.*, “A new interpolation method to measure delta evolution and sediment flux: Application to the late Holocene coastal plain of the Argens River in the western Mediterranean,” *Marine Geology*, vol. 424, p. 106159, 2020, doi: <https://doi.org/10.1016/j.margeo.2020.106159>.
- [16] M. Pratellesi, P. Ciavola, Roberta. Ivaldi, E. J. Anthony, and C. Armaroli, “River-mouth geomorphological changes over >130 years (1882–2014) in a small Mediterranean delta: Is the Magra delta reverting to an estuary?,” *Marine Geology*, vol. 403, pp. 215–224, 2018, doi: <https://doi.org/10.1016/j.margeo.2018.06.003>.
- [17] J. Ericson, C. Vörösmarty, S. Dingman, L. Ward, and M. Meybeck, “Effective Sea-level Rise and Deltas: Causes of Change and Human Dimension Implications,” *Global and Planetary Change*, vol. 50, pp. 63–82, Feb. 2006, doi: 10.1016/j.gloplacha.2005.07.004.
- [18] J. P. M. Syvitski *et al.*, “Sinking deltas due to human activities,” *Nature Geoscience*, vol. 2, no. 10, pp. 681–686, 2009, doi: 10.1038/ngeo629.
- [19] Z. D. Tessler, C. J. Vörösmarty, M. Grossberg, I. Gladkova, and H. Aizenman, “A global empirical typology of anthropogenic drivers of environmental change in deltas,” *Sustainability Science*, vol. 11, no. 4, pp. 525–537, 2016, doi: 10.1007/s11625-016-0357-5.
- [20] S. K. Dolan, R., Hayden, P.B., May, P., May, “The reliability of shoreline change measurements from aerial photographs.,” *Shore Beach*, vol. 48, pp. 22–29, 1980.
- [21] E. H. Boak, I. L. Turner, “Shoreline Definition and Detection: A Review,” *Journal of Coastal Research*, vol. 21, no. 4 (214), pp. 688–703, Jul. 2005, doi: 10.2112/03-0071.1.
- [22] D. Di Luccio *et al.*, “Monitoring and modelling coastal vulnerability and mitigation proposal for an archaeological site (Kaulonia, Southern Italy),” *Sustainability (Switzerland)*, vol. 10, no. 6, pp. 1–18, 2018, doi: 10.3390/su10062017.
- [23] J. T. Kelly and A. M. Gontz, “Using GPS-surveyed intertidal zones to determine the validity of shorelines automatically mapped by Landsat water indices,” *International Journal of Applied Earth Observation and Geoinformation*, vol. 65, no. March 2017, pp. 92–104, 2018, doi: 10.1016/j.jag.2017.10.007.
- [24] K. Vos, M. D. Harley, K. D. Splinter, J. A. Simmons, and I. L. Turner, “Sub-annual to multi-decadal shoreline variability from publicly available satellite imagery,” *Coastal Engineering*, vol. 150, no. April, pp. 160–174, 2019, doi: 10.1016/j.coastaleng.2019.04.004.
- [25] W. Li and P. Gong, “Continuous monitoring of coastline dynamics in western Florida with a 30-year time series of Landsat imagery,” *Remote Sensing of Environment*, vol. 179, pp. 196–209, 2016, doi: 10.1016/j.rse.2016.03.031.
- [26] G. García-Rubio, D. Huntley, and P. Russell, “Evaluating shoreline identification using optical satellite images,” *Marine Geology*, vol. 359, pp. 96–105, 2015, doi: 10.1016/j.margeo.2014.11.002.

- [27] R. S. Dewi and W. Bijker, “Dynamics of shoreline changes in the coastal region of Sayung, Indonesia,” *Egyptian Journal of Remote Sensing and Space Science*, vol. 23, no. 2, pp. 181–193, 2020, doi: 10.1016/j.ejrs.2019.09.001.
- [28] M. A. Kabir, M. Salauddin, K. T. Hossain, I. A. Tanim, M. M. H. Saddam, and A. U. Ahmad, “Assessing the shoreline dynamics of Hatiya Island of Meghna estuary in Bangladesh using multiband satellite imageries and hydro-meteorological data,” *Regional Studies in Marine Science*, vol. 35, p. 101167, 2020, doi: 10.1016/j.rsma.2020.101167.
- [29] S. J. Pitman, D. E. Hart, and M. H. Katurji, “Application of UAV techniques to expand beach research possibilities: A case study of coarse clastic beach cusps,” *Continental Shelf Research*, vol. 184, no. April, pp. 44–53, 2019, doi: 10.1016/j.csr.2019.07.008.
- [30] M. M. Mahabot *et al.*, “The basics for a permanent observatory of shoreline evolution in tropical environments; lessons from back-reef beaches in La Reunion Island,” *Comptes Rendus - Geoscience*, vol. 349, no. 6–7, pp. 330–340, 2017, doi: 10.1016/j.crte.2017.09.010.
- [31] F. Nunziata, A. Buono, M. Migliaccio, G. Benassai, and D. Di Luccio, “Shoreline erosion of microtidal beaches examined with UAV and remote sensing techniques,” *2018 IEEE International Workshop on Metrology for the Sea; Learning to Measure Sea Health Parameters, MetroSea 2018 - Proceedings*, pp. 162–166, 2019, doi: 10.1109/MetroSea.2018.8657843.
- [32] T. Templin, D. Popielarczyk, and R. Kosecki, “Application of Low-Cost Fixed-Wing UAV for Inland Lakes Shoreline Investigation,” *Pure and Applied Geophysics*, vol. 175, no. 9, pp. 3263–3283, 2018, doi: 10.1007/s00024-017-1707-7.
- [33] J. R. Mackenzie, N. C. Duke, and A. L. Wood, “The Shoreline Video Assessment Method (S-VAM): Using dynamic hyperlapse image acquisition to evaluate shoreline mangrove forest structure, values, degradation and threats,” *Marine Pollution Bulletin*, vol. 109, no. 2, pp. 751–763, 2016, doi: 10.1016/j.marpolbul.2016.05.069.
- [34] C. Bouvier, Y. Balouin, and B. Castelle, “Video monitoring of sandbar-shoreline response to an offshore submerged structure at a microtidal beach,” *Geomorphology*, vol. 295, no. January, pp. 297–305, 2017, doi: 10.1016/j.geomorph.2017.07.017.
- [35] J. Moussaid, A. A. Fora, B. Zourarah, M. Maanan, and M. Maanan, “Using automatic computation to analyze the rate of shoreline change on the Kenitra coast, Morocco,” *Ocean Engineering*, vol. 102, pp. 71–77, 2015, doi: 10.1016/j.oceaneng.2015.04.044.
- [36] M. Bini, N. Casarosa, and A. Ribolini, “L’evoluzione diacronica della linea di riva del litorale Pisano (1938-2004) sulla base del confronto di immagini aeree georeferenziate,” *Atti della Società Toscana di Scienze Naturali, Memorie Serie A*, vol. 113, no. January 2008, pp. 1–12, 2008.
- [37] N. G. Plant and R. A. Holman, “Intertidal beach profile estimation using video images,” *Marine Geology*, vol. 140, no. 1, pp. 1–24, 1997, doi: [https://doi.org/10.1016/S0025-3227\(97\)00019-4](https://doi.org/10.1016/S0025-3227(97)00019-4).
- [38] R. K. Smith and K. R. Bryan, “Monitoring Beach Face Volume with a Combination of Intermittent Profiling and Video Imagery,” *Journal of Coastal Research*, vol. 2007, no. 234, pp. 892–898, Jul. 2007, doi: 10.2112/04-0287.1.

- [39] Federici and Mazzanti, *Note sulle pianure costiere della Toscana*. Roma, 1993.
- [40] E. Pranzini, “Updrift river mouth migration on cusped deltas: two examples from the coast of Tuscany (Italy),” *Geomorphology*, vol. 38, no. 1, pp. 125–132, 2001, doi: [https://doi.org/10.1016/S0169-555X\(00\)00076-3](https://doi.org/10.1016/S0169-555X(00)00076-3).
- [41] G. Sarti, M. Bini, and S. Giacomelli, “The growth and the decline of Pisa (Tuscany, Italy) up to the Middle ages: correlations with landscape and geology,” *Quat. Ital. J. Quat. Sci.*, vol. 23, pp. 311–322, Oct. 2010.
- [42] M. Bini *et al.*, “Palaeoenvironments and palaeotopography of a multilayered city during the Etruscan and Roman periods: early interaction of fluvial processes and urban growth at Pisa (Tuscany, Italy),” *Journal of Archaeological Science*, vol. 59, pp. 197–210, 2015, doi: <https://doi.org/10.1016/j.jas.2015.04.005>.
- [43] R. Mazzanti, *La pianura pisana e i rilievi contermini*. 1994.
- [44] E. Pranzini, “Updrift river mouth migration on cusped deltas: two examples from the coast of Tuscany (Italy),” *Geomorphology*, vol. 38, no. 1, pp. 125–132, 2001, doi: [https://doi.org/10.1016/S0169-555X\(00\)00076-3](https://doi.org/10.1016/S0169-555X(00)00076-3).
- [45] G. Sarti, M. Bini, and S. Giacomelli, “The growth and the decline of Pisa (Tuscany, Italy) up to the Middle ages: correlations with landscape and geology,” *Quat. Ital. J. Quat. Sci.*, vol. 23, pp. 311–322, Oct. 2010.
- [46] M. Bini *et al.*, “Palaeoenvironments and palaeotopography of a multilayered city during the Etruscan and Roman periods: early interaction of fluvial processes and urban growth at Pisa (Tuscany, Italy),” *Journal of Archaeological Science*, vol. 59, pp. 197–210, 2015, doi: <https://doi.org/10.1016/j.jas.2015.04.005>.
- [47] G. Sarti *et al.*, “Climatic signature of two mid–late Holocene fluvial incisions formed under sea-level highstand conditions (Pisa coastal plain, NW Tuscany, Italy),” *Palaeogeography, Palaeoclimatology, Palaeoecology*, vol. 424, pp. 183–195, 2015, doi: <https://doi.org/10.1016/j.palaeo.2015.02.020>.
- [48] A. R. Toniolo, *Sulle Variazioni di spiaggia a foce d’Arno (Marina di Pisa) dalla fine del secolo XVIII ai nostri giorni: Studio storico fisiografico*. Pisa: Tipografia Municipale, 1910.
- [49] E. Pranzini, G. Anfuso, I. Cinelli, M. Piccardi, and G. Vitale, “Shore protection structures increase and evolution on the Northern Tuscany Coast (Italy): Influence of tourism industry,” *Water (Switzerland)*, vol. 10, no. 11, 2018, doi: [10.3390/w10111647](https://doi.org/10.3390/w10111647).
- [50] N. Casarosa, “Studio dell’evoluzione del litorale pisano tramite rilievi con GPS differenziale (2008-2014),” *Studi costieri*, pp. 3–19, 2016.
- [51] M. Bini, N. Casarosa, and M. Luppichini, “Exploring the relationship between river discharge and coastal erosion: An integrated approach applied to the pisa coastal plain (italy),” *Remote Sensing*, vol. 13, no. 2, 2021, doi: [10.3390/rs13020226](https://doi.org/10.3390/rs13020226).
- [52] Autorità di bacino del Fiume Arno, “Attività estrattive,” in *Supplemento alla Gazzetta Ufficiale, Serie Generale n. 122*, 2000.
- [53] P. Billi and M. Rinaldi, “Human impact on sediment yield and channel dynamics in the Arno River Basin (central Italy),” *Human impact on erosion and sedimentation. Proc. international symposium, Rabat, Morocco, 1997*, vol. 245, no. 245, pp. 301–311, 1997.
- [54] P. Aminti, C. Cammelli, L. Cappietti, N. L. Jackson, K. F. Nordstrom, and E. Pranzini, “Evaluation of Beach Response to Submerged Groin Construction at

- Marina di Ronchi, Italy, Using Field Data and a Numerical Simulation Model,” *Journal of Coastal Research*, pp. 99–120, Sep. 2004, [Online]. Available: <http://www.jstor.org/stable/25736248>
- [55] M. Bini, N. Casarosa, and A. Ribolini, “L’evoluzione diacronica della linea di riva del litorale Pisano (1938-2004) sulla base del confront di immagini aeree georeferenziate,” *Atti della Societa Toscana di Scienze Naturali, Memorie Serie A*, vol. 113, no. January 2008, pp. 1–12, 2008.
- [56] E. Pranzini and D. Simonetti, “Influenza del fattore scala sulla classificazione delle spiagge in base alla loro tendenza evolutiva,” *Studi costieri*, vol. 14, pp. 13–28, 2008.
- [57] D. G. Lowe, “Distinctive Image Features from Scale-Invariant Keypoints,” *International Journal of Computer Vision*, vol. 60, no. 2, pp. 91–110, 2004, doi: 10.1023/B:VISI.0000029664.99615.94.
- [58] M. J. Westoby, J. Brasington, N. F. Glasser, M. J. Hambrey, and J. M. Reynolds, ““Structure-from-Motion” photogrammetry: A low-cost, effective tool for geoscience applications,” *Geomorphology*, vol. 179, pp. 300–314, 2012, doi: <https://doi.org/10.1016/j.geomorph.2012.08.021>.
- [59] M. Favalli, A. Fornaciai, I. Isola, S. Tarquini, and L. Nannipieri, “Multiview 3D reconstruction in geosciences,” *Computers & Geosciences*, vol. 44, pp. 168–176, 2012, doi: <https://doi.org/10.1016/j.cageo.2011.09.012>.
- [60] D. Bertoni, G. Sarti, F. Alquini, and D. Ciccarelli, “Implementing a coastal dune vulnerability index (CDVI) to support coastal management in different settings (Brazil and Italy),” *Ocean and Coastal Management*, vol. 180, 2019, doi: 10.1016/j.ocecoaman.2019.104916.
- [61] M. Kohv, E. Sepp, and L. Vammus, “Assessing multitemporal water-level changes with uav-based photogrammetry,” *The Photogrammetric Record*, vol. 32, no. 160, pp. 424–442, Dec. 2017, doi: 10.1111/phor.12214.
- [62] M. Luppichini, M. Bini, M. Paterni, A. Berton, and S. Merlino, “A new beach topography-based method for shoreline identification,” *Water (Switzerland)*, vol. 12, no. 11, pp. 1–11, Nov. 2020, doi: 10.3390/w12113110.
- [63] K. Vos, M. D. Harley, K. D. Splinter, J. A. Simmons, and I. L. Turner, “Sub-annual to multi-decadal shoreline variability from publicly available satellite imagery,” *Coastal Engineering*, vol. 150, no. April, pp. 160–174, 2019, doi: 10.1016/j.coastaleng.2019.04.004.
- [64] G. García-Rubio, D. Huntley, and P. Russell, “Evaluating shoreline identification using optical satellite images,” *Marine Geology*, vol. 359, pp. 96–105, 2015, doi: 10.1016/j.margeo.2014.11.002.
- [65] E. Sánchez-García, J. E. Pardo-Pascual, A. Balaguer-Beser, and J. Almonacid-Caballer, “Analysis of the shoreline position extracted from landsat TM and ETM+ imagery,” *International Archives of the Photogrammetry, Remote Sensing and Spatial Information Sciences - ISPRS Archives*, vol. 40, no. 7W3, pp. 991–998, 2015, doi: 10.5194/isprsarchives-XL-7-W3-991-2015.